Relative motion of transmembrane segments S0 and S4 during voltage sensor activation in the human BK_{Ca} channel

Antonios Pantazis,[1] Azadeh P. Kohanteb,[1] and Riccardo Olcese[1,2,3]

[1]Department of Anesthesiology, Division of Molecular Medicine, [2]Brain Research Institute, and [3]Cardiovascular Research Laboratories, David Geffen School of Medicine, University of California, Los Angeles, Los Angeles, CA 90075

Large-conductance voltage- and Ca^{2+}-activated K^+ (BK_{Ca}) channel α subunits possess a unique transmembrane helix referred to as S0 at their N terminus, which is absent in other members of the voltage-gated channel superfamily. Recently, S0 was found to pack close to transmembrane segments S3 and S4, which are important components of the BK_{Ca} voltage-sensing apparatus. To assess the role of S0 in voltage sensitivity, we optically tracked protein conformational rearrangements from its extracellular flank by site-specific labeling with an environment-sensitive fluorophore, tetramethylrhodamine maleimide (TMRM). The structural transitions resolved from the S0 region exhibited voltage dependence similar to that of charge-bearing transmembrane domains S2 and S4. The molecular determinant of the fluorescence changes was identified in W203 at the extracellular tip of S4: at hyperpolarized potential, W203 quenches the fluorescence of TMRM labeling positions at the N-terminal flank of S0. We provide evidence that upon depolarization, W203 (in S4) moves away from the extracellular region of S0, lifting its quenching effect on TMRM fluorescence. We suggest that S0 acts as a pivot component against which the voltage-sensitive S4 moves upon depolarization to facilitate channel activation.

INTRODUCTION

Large-conductance voltage- and Ca^{2+}-activated K^+ (BK_{Ca} or MaxiK) channels are ubiquitous membrane proteins that potently regulate cellular excitability (Toro et al., 1998; Latorre and Brauchi, 2006; Salkoff et al., 2006; Wu and Marx, 2010). BK_{Ca} channels are formed by α subunit homotetramers, each comprising a conserved transmembrane voltage-sensing domain (VSD), a pore domain, and a large intracellular ligand-binding domain (Fig. 1), recently visualized by cryoelectron microscopy (Wang and Sigworth, 2009). BK_{Ca} channels possess several unique features that set them apart from other voltage-gated ion channels. First, as their name suggests, they exhibit an exceptionally high conductance for K^+, over an order of magnitude greater than that of other voltage-gated K^+ channels (Latorre and Miller, 1983). Second, they are activated by the allosteric interplay of membrane depolarization and Ca binding (Cui and Aldrich, 2000; Rothberg and Magleby, 2000; Horrigan and Aldrich, 2002; Magleby, 2003; Latorre and Brauchi, 2006; Sweet and Cox, 2008; Cui et al., 2009; Latorre et al., 2010; Lee and Cui, 2010). Ca is thought to bind with high affinity to the cytosolic domain (Wei et al., 1994; Schreiber and Salkoff, 1997; Bian et al., 2001; Braun and Sy, 2001; Xia et al., 2002; Bao et al., 2004; Sheng et al., 2005; Zeng et al., 2005; Yusifov et al.,

2008, 2010; Yang et al., 2010; Yuan et al., 2010), which is also sensitive to other ligands and biological partners that modulate channel activation (Lu et al., 2006; Hou et al., 2009; Cui, 2010).

Another unique aspect of BK_{Ca} channels is their transmembrane topology: a typical voltage-gated K^+ channel α subunit crosses the membrane six times; the four most N-terminal helical transmembrane segments (S1–S4) comprise the VSD, whereas S5 and S6 contribute to the central ion-selective pore (Armstrong, 2003; Swartz, 2004; Long et al., 2005, 2007) (Fig. 1). BK_{Ca} channel α subunits possess an additional transmembrane domain, S0, which renders their N-terminal tail extracellular (Wallner et al., 1996; Meera et al., 1997; Morrow et al., 2006). S0 and the extracellular N-terminal flank are required for the functional interaction between channel-forming α subunits and accessory β subunits (Wallner et al., 1996; Morrow et al., 2006; Liu et al., 2008b, 2010; Wu et al., 2009), which modulate the channel activation mechanism and, because of their subtype-restricted expression pattern, confer tissue-specific effects to BK_{Ca} channel function (Orio et al., 2002, 2006; Bao and Cox, 2005; Orio and Latorre, 2005; Savalli et al., 2007; Sweet and Cox, 2009; Latorre et al., 2010; Wu and Marx, 2010).

The Rockefeller University Press $30.00
J. Gen. Physiol. Vol. 136 No. 6 645–657
www.jgp.org/cgi/doi/10.1085/jgp.201010503

645

Because S0 is a unique transmembrane feature of BK_{Ca} channels with little homology to the N termini of other K_V channels, its position and orientation relative to other transmembrane segments, as well as its precise boundaries, cannot be inferred from a direct comparison with K_V channel crystal structures available to date. Its hydropathy profile indicates that its hydrophobic transmembrane portion spans residues Met-21 to Trp-43 and is flanked by arginines at positions 20 and 44 (Wallner et al., 1996; Morrow et al., 2006). Tryptophan substitution at specific positions in S0 impairs BK_{Ca} channel voltage sensing, presumably because they perturb a site of interaction between S0 and the VSD (Koval et al., 2007). Indeed, studies based on disulfide bridge formation efficiency determined that S0 is highly associated with segments S3 and S4 (Liu et al., 2008a, 2010),

both of which possess voltage-sensing charged residues and are thus key components of the BK_{Ca} voltage-sensing apparatus (Stefani et al., 1997; Díaz et al., 1998; Cui and Aldrich, 2000; Ma et al., 2006; Savalli et al., 2006; Pantazis et al., 2010).

If S0 is indeed intimately associated with the BK_{Ca} voltage-sensing apparatus, then S0 or its immediate proximity should undergo voltage-dependent transitions. We have previously used the voltage clamp fluorometry method (Gandhi and Isacoff, 2005; Claydon and Fedida, 2007; Gandhi and Olcese, 2008; Horne and Fedida, 2009) to optically resolve the voltage-dependent transitions of S2 and S4 in the BK_{Ca} VSD (Savalli et al., 2006, 2007; Pantazis et al., 2010). In this work, we sought to probe the role of S0 in the BK_{Ca} VSD by resolving protein rearrangements in its immediate proximity.
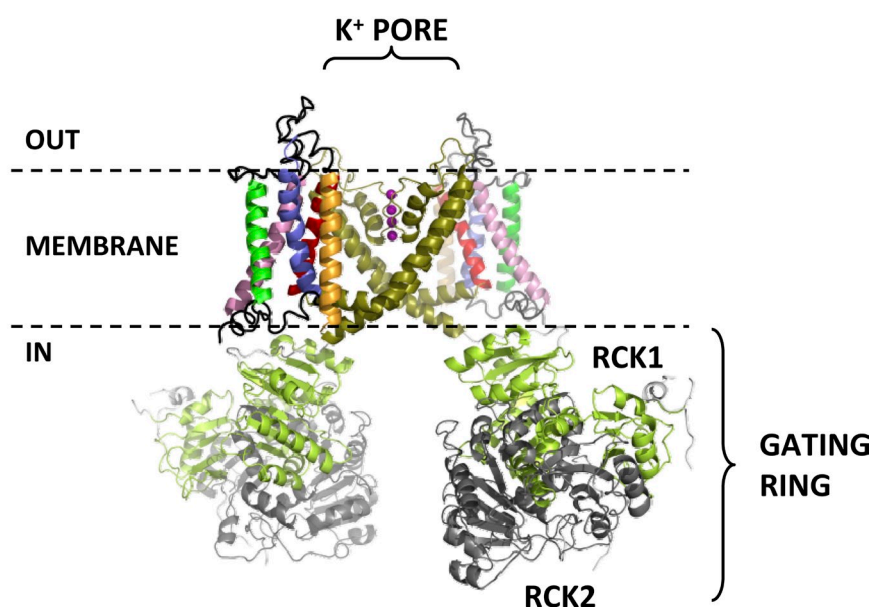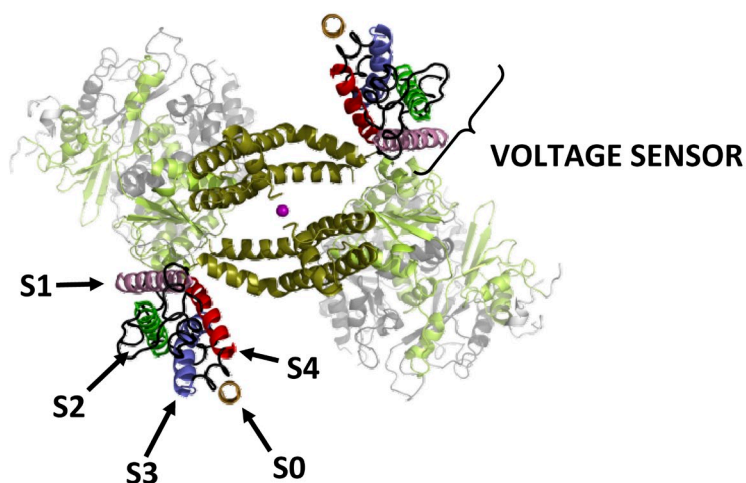

Figure 1. Side and top views of the putative structure of the BK_{Ca} channel. Only two out of four α subunits are shown for clarity. Each α subunit consists of seven transmembrane segments (S0–S6) and a large intracellular ligand-binding domain. Segments S0–S4 comprise the VSD, whereas segments S5 and S6 from all four subunits contribute to the central, K^+-selective pore (K^+ ions occupying the pore are shown as purple spheres). Each subunit also contributes an intracellular RCK1/RCK2 heterodimer, which assembles into the hetero-octameric gating ring superstructure. The structure shown for domains S1–S6 is from the atomic structure of the K_V1.2-2.1 chimera (Protein Data Bank accession no. 2R9R) (Long et al., 2007); S0 was modeled as an ideal α helix. Note its close association with voltage-sensing segments S3 and S4, as recently suggested by Liu et al. (2010). The intracellular domain structures (available from Protein Data Bank accession no. 3NAF) (Wu et al., 2010) were manually docked on the 2R9R structure.

The central principle of voltage clamp fluorometry is that many fluorophores are sensitive to nearby environmental factors, such as hydropathy, quenching groups, etc. (Lakowicz, 2006). By engineering such fluorophores with a sulfhydryl-reactive moiety, such as maleimide, it is possible to covalently attach them to a specific position of the protein where a unique cysteine has been introduced. If this area of the protein then undergoes movement upon depolarization that causes a change of the fluorophore environment, a deflection in the fluorescence intensity will be observed. This technique was pioneered in Shaker K^{+} channels (Mannuzzu et al., 1996; Cha and Bezanilla, 1997) and has since been used to probe the voltage-dependent operation of other K_V channels (Smith and Yellen, 2002; Bannister et al., 2005; Vaid et al., 2008; Horne et al., 2010), Na_V channels (Chanda and Bezanilla, 2002), HCN channels, (Bruening-Wright et al., 2007), H_V channels (Tombola et al., 2010), and the VSD-activated phosphatase, *Ci*-VSP (Kohout et al., 2008; Villalba-Galea et al., 2008).

By combining this approach with the quenching properties of a tryptophan residue in the extracellular tip of S4, we optically resolved a voltage-dependent divergence of the extracellular portions of S0 and S4: a direct demonstration of protein segments rearranging relative to each other during activation. In this context, we speculate that S0 could act as a pivot element, closely associated with the voltage-sensing S4 at rest; however, upon membrane depolarization, S4 moves against and away from S0 to facilitate channel activation.

MATERIALS AND METHODS

Molecular biology
For site-directed fluorescence labeling with a thiol-reactive fluorophore, an hSlo clone (no. U11058; provided by L. Toro, University of California, Los Angeles, CA) (Wallner et al., 1995) transcribed from the fourth methionine without extracellular cysteines (C14S, C141S, and C277S) was used. Background mutation R207Q was introduced to increase P_O (Díaz et al., 1998; Ma et al., 2006). A single cysteine was substituted at positions 17, 18, 19, or 20 (outside S0), 145 (outside S2), or 202 (outside S4) to track voltage-dependent conformational transitions from these segments. Single point mutations were generated with QuikChange Site-Directed Mutagenesis kit (Agilent Technologies) and confirmed by sequencing. The cDNAs were translated to cRNAs in vitro (mMESSAGE MACHINE; Applied Biosystems) and stored at −80°C.

Oocyte preparation
Xenopus laevis (Nasco) oocytes (stage V–VI) were prepared as described previously (Haug et al., 2004), and then injected with 50 nl of total cRNA (0.2–0.5 µg/µl) using a nano-injector (Drummond Scientific Company). Injected oocytes were maintained at 18°C in an amphibian saline solution supplemented with 50 µg/ml gentamycin (Invitrogen), 200 µM DTT, and 10 µM EDTA. 3–6 d after injection, oocytes were stained for 30–45 min with 10 µM of a membrane-impermeable, thiol-reactive fluorophore, tetramethylrhodamine-5′-maleimide (TMRM; Invitrogen), in a depo-

larizing K^{+} solution (in mM: 120 K-methanesulfonate [MES], 2 Ca(MES)$_2$, and 10 HEPES, pH 7) at room temperature. TMRM stock (100 mM) was dissolved in DMSO and stored at −20°C. The oocytes were then thoroughly rinsed in a dye-free solution before being mounted in the recording chamber. Changes in fluorescence emission were a result of environmental differences sensed by the fluorophores.

Electrophysiological techniques
The cut-open oocyte voltage clamp. The cut-open oocyte Vaseline gap technique is a low-noise, fast clamp technique (Stefani and Bezanilla, 1998). The oocyte is placed in a triple-compartment Perspex chamber, with a diameter of 600 µm for the top and bottom rings. The top chamber isolates the oocyte's upper domus and maintains it under clamp. The middle chamber provides a guard shield by clamping the middle part of the oocyte to the same potential as the top chamber. The bottom chamber injects current intracellularly through the saponin-permeabilized part of the oocyte. Fluorescence emission and ionic current were simultaneously measured from the same area of membrane isolated by the top chamber (Gandhi and Olcese, 2008). The optical setup consists of a microscope (Axioscope FS; Carl Zeiss, Inc.) with filters (Omega Optical) appropriate for TMRM. The light source is a 100-W microscope halogen lamp. A TTL-triggered shutter (Uniblitz VS 25; Vincent Associates) is mounted on the excitation light path. The objective (40×, water immersion; LUMPlanFl; Olympus) has a numerical aperture of 0.8 and a working distance of 3.3 mm (Olympus), which leaves enough room for the insertion of the microelectrode. The emission light is focused on a photodiode (PIN-08-GL; UDT Technologies). An amplifier (Photomax 200; Dagan) is used for the amplification of the photocurrent and background fluorescence subtraction. The external solution contained (in mM): 110 Na-MES, 10 K-MES, 2 Ca(MES)$_2$, and 10 Na-HEPES, pH 7.0. The internal solution contained (in mM): 120 K-glutamate and 10 HEPES, pH 7.0. Standard solution for the intracellular recording micropipette is (in mM): 2,700 Na-MES and 10 NaCl. Low access resistance to the oocyte interior was obtained by permeabilizing the oocyte with 0.1% saponin carried by the internal solution.

Analysis. Experimental data were analyzed with a customized program developed in our division and using fitting routines run in Microsoft Excel. The G(V) curves were calculated by dividing the current–voltage relationships (I-V curves) by the driving force ($V_m - E_K$), where V_m is the membrane potential and E_K the equilibrium potential for K^{+}, estimated using the Nernst equation. Data for the membrane conductance (G(V)) and the fluorescence (F(V)) curves were fitted to one or two Boltzmann distributions of the form:

$$G(V) = \frac{G_{max}}{1 + e^{\left[z(Vhalf - Vm)\left(\frac{F}{RT}\right)\right]}}$$

$$F(V) = \frac{F_{max} - F_{min}}{1 + e^{\left[z(Vhalf - Vm)\left(\frac{F}{RT}\right)\right]}} - F_{min},$$

where G_{max} and F_{max} are the maximal G and F, F_{min} is the minimal F, z is the effective valence of the distribution, V_{half} is the half-activating potential, V_m is the membrane potential, and F, R, and T are the usual thermodynamic values.

TMRM fluorometry in solution
The fluorescence of TMRM in solution (1 µM dissolved in external solution, pH 7.0) was measured using a spectrofluorometer

(Fluorolog-3; HORIBA): λ_{ex} = 545 nm, 5-nm slit; λ_{em} = 550–650 nm, 1-nm slit. A stock of L-tryptophan analogue N-acetyl-L-tryptophan-amide (NATA; Sigma-Aldrich) was prepared at 40 mM in external solution containing 1 µM TMRM, pH 7.0, and its concentration was ascertained by its absorbance at 280 nm according to its extinction coefficient (5,690 M^{-1}). NATA solution was progressively added to measure its quenching effect on TMRM fluorescence emission. This was quantified according to the Stern-Volmer equation (Lakowicz, 2006):

$$\frac{F_0}{F} = 1 + K_{SV}[\text{NATA}],$$

where F_0 is peak TMRM fluorescence emission (at 573 nm) without NATA, F is the peak of TMRM fluorescence emission peak (573 nm) with NATA, K_{SV} is the Stern-Volmer quenching constant, and [NATA] is NATA concentration.

Online supplemental material

Fig. S1 shows a proposed mechanism to account for the composite fluorescence signal reported from position 20. This scheme explains how two distinct quenching processes can generate the observed fluorescence signal. It is available at http://www.jgp.org/cgi/content/full/jgp.201010503/DC1.

RESULTS

The extracellular flank of S0 experiences environmental changes during voltage-dependent channel activation

Recent studies have proposed that S0 closely associates with the voltage-sensing apparatus (Koval et al., 2007; Liu et al., 2008a, 2010), raising the prospect of its involvement in VSD operation. To investigate this hypothesis we sought to optically track voltage-dependent conformational rearrangements from its extracellular flank. A cysteine residue was substituted into position 17, 18, or 19 in a human BK_{Ca} channel α subunit clone (hSlo) devoid of native extracellular cysteines (Cless).
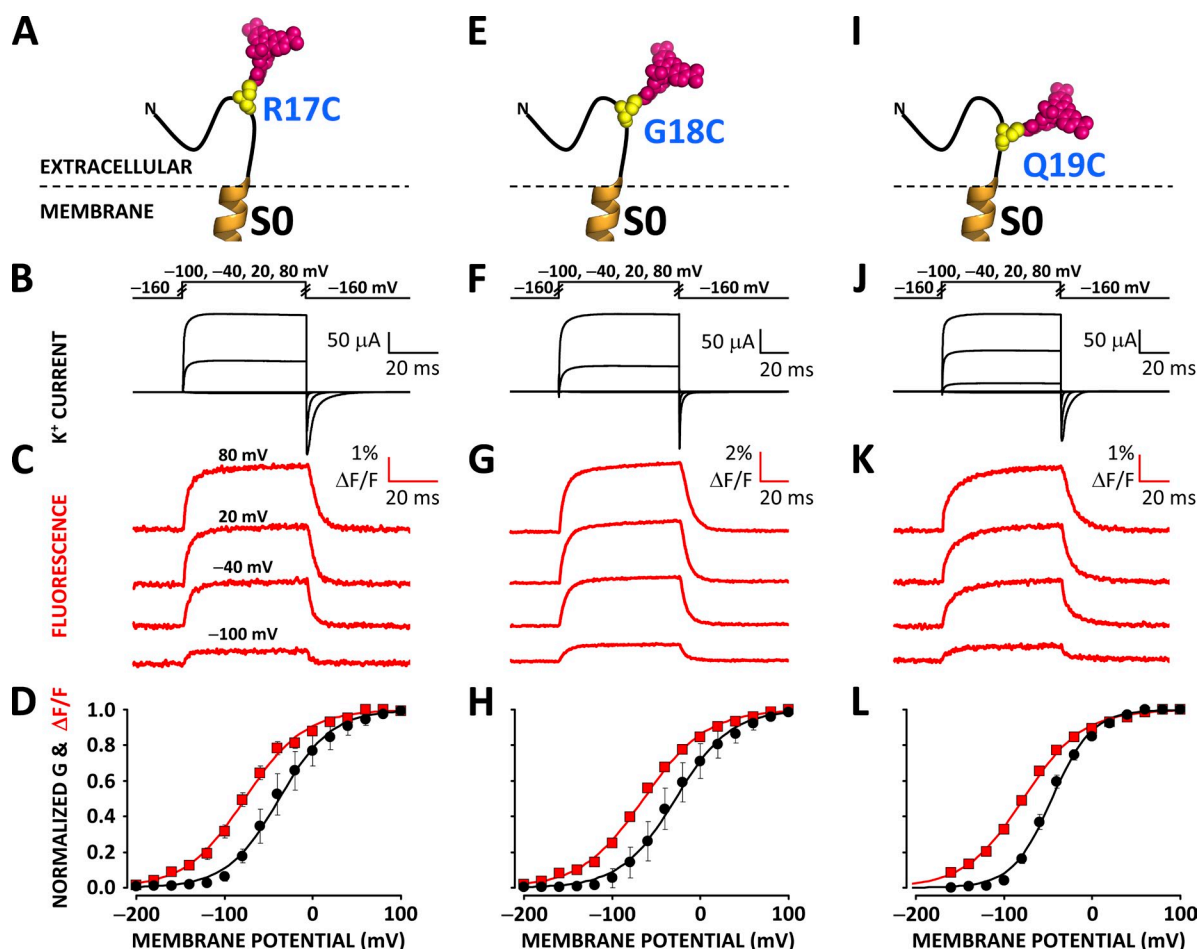

Figure 2. Voltage-dependent conformational rearrangements reported from the N-terminal flank of S0. (A) A unique cysteine was substituted at position 17 at the putative N-terminal flank of S0 in a BK_{Ca} channel α subunit and covalently labeled with the fluorophore TMRM to resolve conformational rearrangements from this region. (B) Voltage pulses and characteristic evoked K^+ currents from BK_{Ca} channels labeled with TMRM at position 17. (C) TMRM fluorescence traces recorded during the voltage pulses in B. (D) Normalized K^+ conductance (G; black circles) and $\Delta F/F$ (red squares) plotted against membrane potential and fitted with Boltzmann distributions (black and red curves, respectively). Boltzmann parameters are listed in Table I. Error bars represent SEM. (E–H) As in A–D, respectively, for BK_{Ca} channels labeled with TMRM at position 18. (I–L) As in A–D, respectively, for BK_{Ca} channels labeled with TMRM at position 19.

The mutation R207Q was also introduced to increase P_O at low [Ca] (Díaz et al., 1998). *Xenopus* oocytes expressing these channels were incubated with the environment-sensitive fluorophore TMRM, which covalently bound to the engineered cysteine (Fig. 2, A, E, and I). The labeled oocytes were mounted on a cut-open oocyte Vaseline gap voltage clamp setup modified for epifluorescence measurement to simultaneously record ionic current (Fig. 2, B, F, and J) and fluorescence emission. Pronounced voltage-dependent fluorescence deflections ($\Delta F/F$), which underlie protein rearrangements, were reported from all tested positions (17, 18, and 19) on the extracellular flank of S0 (Fig. 2, C, G, and K). The similarity in time course, amplitude, and voltage dependence (Table I) of the fluorescence deflections resolved from position 17, 18, or 19 suggests that fluorophores at these three sites track the same molecular process. Their voltage dependence is indeed similar to that of protein rearrangements reported from voltage-sensing segments S2 and S4 (Savalli et al., 2006; Pantazis et al., 2010) (Table I), suggesting a process related to the operation of the BK_{Ca} voltage sensor.

Is S0 a voltage-sensing component of the BK_{Ca} VSD?

The conformational rearrangements reported from positions 17, 18, and 19 could imply a voltage-dependent movement of S0. To undergo voltage-dependent motion, a transmembrane segment needs to either possess voltage-sensing charge(s) (i.e., charged residues experi-

encing the membrane electric field; Tombola et al., 2006; Bezanilla, 2008; Chanda and Bezanilla, 2008; Swartz, 2008) or interact with another voltage-sensing segment. According to the hydropathy profile of S0, a positively charged arginine at position 20 maps at the interface between the membrane and the extracellular solution, whereas another arginine, R44, defines the putative cytosolic flank of S0 (Wallner et al., 1996; Meera et al., 1997).

Accordingly, R20 could either experience a fraction of the membrane electric field or be involved in electrostatic interactions with charged residues in another voltage-sensing segment. We have investigated the voltage dependence of protein rearrangements and ionic conductance in channels bearing mutation R20A and labeled at S0 (Fig. 3 A), S2 (Fig. 3 F), or S4 (Fig. 3 K). R20A mutants exhibited a positive shift in the voltage dependence of ionic conductance by ≈30 mV (Fig. 3, D, I, and N, and Table I). The voltage dependence of conformational rearrangements reported from S0, S2, and S4 exhibited a shift in the same direction (Fig. 3 E, J, and O, and Table I). However, although the R20A mutation appeared to perturb the voltage-dependent activation of BK_{Ca} channels, it failed to significantly reduce the voltage dependence of the conformational rearrangements reported from S0. That is, the effective valence (z) of $\Delta F/F$ resolved from S0-labeled channels was not significantly reduced by mutation R20A (Table I). In contrast, voltage-sensing charge neutralization within BK_{Ca} S2 and S4 domains reduced the effective valence

TABLE I

Boltzmann fitting parameters for conductance and fluorescence data from TMRM-labeled BK_{Ca} channel clones

Clone	Conductance		Fluorescence		n
hSlo-Cless-R207Q-	V_{half}	z	V_{half}	z	
	(mV)	*(e^0)*	*(mV)*	*(e^0)*	
R17C	-36 ± 12	1.1 ± 0.20	-72 ± 7.6	0.89 ± 0.11	16
R17C-R20A	-7.7 ± 1.8	0.75 ± 0.06	-52 ± 3.0	0.61 ± 0.02	3
R17C-W203V	29 ± 3.3	1.0 ± 0.02	-74 ± 2.5	0.51 ± 0.02	6
G18C	-25 ± 13	1.2 ± 0.24	-64 ± 3.6	0.75 ± 0.03	18
G18C-R20A	5.6 ± 7.5	0.91 ± 0.11	-32 ± 3.2	0.75 ± 0.02	5
G18C-W203V	18 ± 7.2	0.96 ± 0.05	-88 ± 6	0.68 ± 0.05	8
Q19C	-45 ± 3.5	1.3 ± 0.06	-78 ± 3.3	0.81 ± 0.03	18
Q19C-R20A	-7.2 ± 9.7	0.85 ± 0.06	-59 ± 4.6	0.85 ± 0.03	9
Q19C-W203V	13 ± 9.2	0.93 ± 0.05	-94 ± 11	0.65 ± 0.07	7
R20C	-30 ± 7.5	1.4 ± 0.13	N/A	N/A	13
R20C-W203V	10 ± 12	1.0 ± 0.07	-61 ± 5.0	0.86 ± 0.03	6
Y145C	-26 ± 10	1.2 ± 0.11	-82 ± 5.0	0.74 ± 0.05	14
Y145C-R20A	0 ± 10	1.1 ± 0.11	-43 ± 6.1	0.58 ± 0.03	10
Y145C-W203V[a]	9.9 ± 2.2	0.86 ± 0.10	-58 ± 9.3	0.57 ± 0.05	8
S202C[b]	-46	1.29	-75	1.20	
S202C-W203V[a,b]	1.9 ± 4.0	0.98 ± 0.03	-70 ± 2.6	0.66 ± 0.04	18
S202C-R20A-W203V	29 ± 5.3	0.99 ± 0.05	-51 ± 7.2	0.53 ± 0.02	13

Labeling positions: R17C, G18C, Q19C, R20C: S0/N-terminus; Y145C: extracellular to S2; S202C: S3/S4 linker. Errors are ± SEM.
[a]Pantazis et al., 2010.
[b]Savalli et al., 2006.

of these segments by ≈70% (Pantazis et al., 2010). These results suggest that R20 is not responsible for the voltage-dependent motions reported from the extracellular flank of S0; it is therefore unlikely to have a role as a voltage-sensing charge.

We did not achieve functional channel expression in a channel bearing the mutation R44A or R44Q at the cytosolic tip of S0, preventing a further characterization of the role of this charge in the wild-type (wt) channel.

Two distinct molecular events can be resolved by labeling position 20

To better characterize the nature of the conformational rearrangements detected from S0, we labeled position 20 (R20C) with TMRM (Fig. 4 A). The fluorescence deflections resolved from this position are intriguing in that they exhibit two distinct components: upon depolarization, the fluorescence is initially quenched (Fig. 4 F, state 1), followed by unquenching (state 2). Upon repolarization, the fluorescence is transiently unquenched
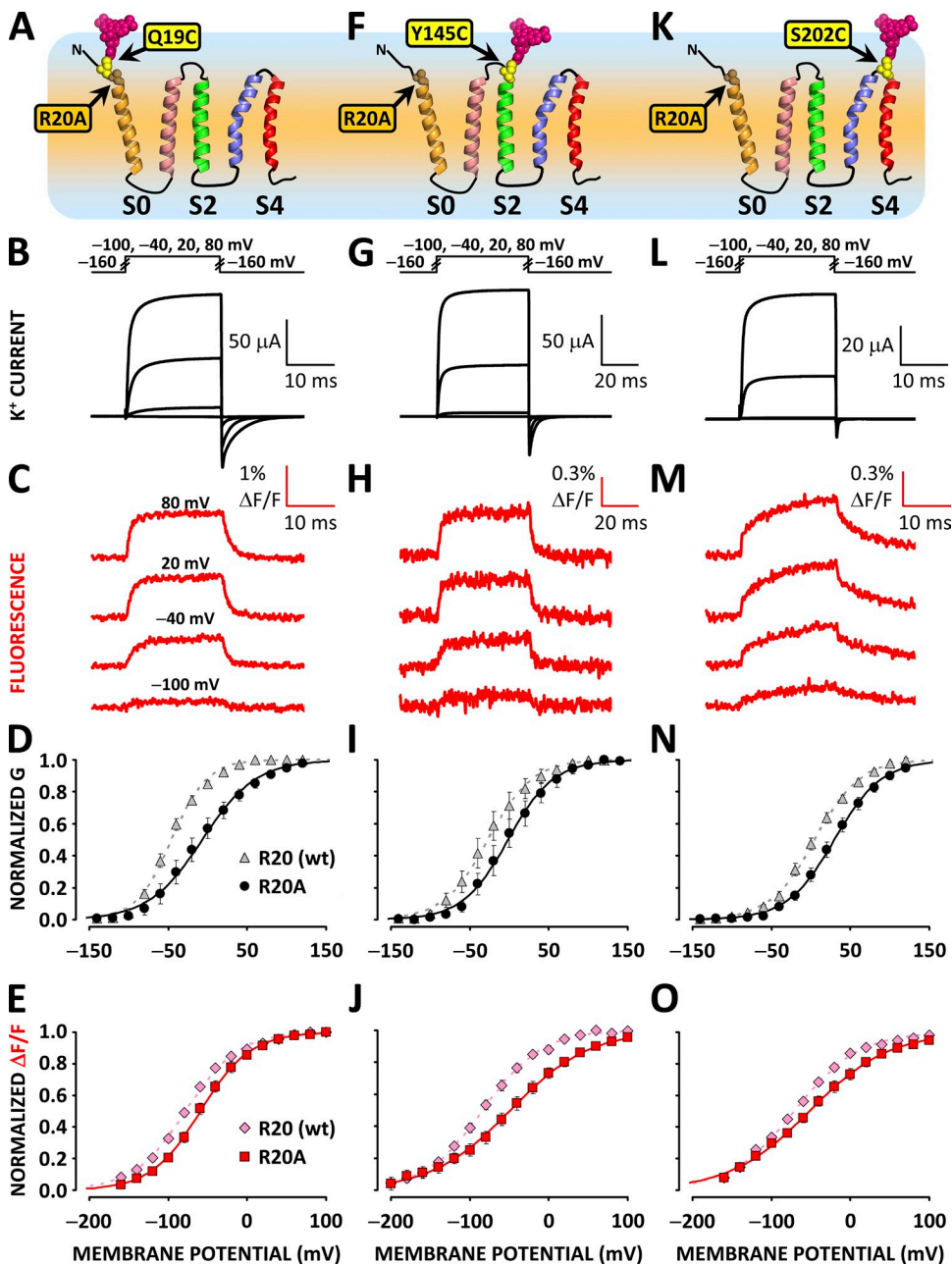

Figure 3. Neutralization of R20 alters channel activation but does not prevent conformational rearrangements reported from the S0 region. (A) Putative topology of the BK$_{Ca}$ channel α subunit voltage sensor domain. A unique cysteine was substituted at position 19 at the putative N-terminal flank of S0, bearing mutation R20A and covalently labeled with the fluorophore TMRM to resolve conformational rearrangements from this region. (B) Voltage pulses and characteristic evoked K$^+$ currents from R20A BK$_{Ca}$ channels labeled with TMRM at position 19. (C) TMRM fluorescence traces recorded during the voltage pulses in B. (D) Normalized K$^+$ conductance from channels with mutation R20A (black circles) and without (gray triangles) plotted against membrane potential and fitted with Boltzmann distributions (black and gray curves, respectively). Boltzmann parameters are listed in Table I. Error bars represent SEM. (E) Normalized TMRM fluorescence from channels with mutation R20A (red squares) and without (pink diamonds), plotted against membrane potential and fitted with Boltzmann distributions (red and pink curves, respectively). Boltzmann parameters are listed in Table I. Error bars represent SEM. (F–J) As in A–E, respectively, for BK$_{Ca}$ channels labeled with TMRM at position 145 at the extracellular tip of S2. (K–O) As in A–E, respectively, for BK$_{Ca}$ channels labeled with TMRM at position 202 at the short extracellular linker between segments S3 and S4.

Mutation W203V was included to enhance ΔF/F signals from position 202 (Savalli et al., 2006). Mutation R20A impaired the activation of all TMRM-labeled BK$_{Ca}$ channels investigated, as it shifted the midpoint of activation (V_{half}) toward depolarized potentials by ≈30 mV (see Table I).

further (state 3), followed by return to resting state (state 0). Thus, TMRM-labeled position 20 reports two kinetically distinct processes with opposite effects on the fluorescence emission. The two processes also possess different voltage dependence at steady state: for voltage steps up to −60 mV, only the quenching component is evident, as shown by the downward fluorescence deflections (Fig. 4 C). However, for higher test potentials, the unquenching process becomes prominent, resulting in an overall positive fluorescence deflection (Fig. 4, C and F). As such, the steady-state F-V relationship is a convolution of two processes with opposite effects on fluorophore emission and distinct voltage dependence (Fig. 4 E). An implication of the fluorescence at position 20 tracking two processes with distinct kinetics and voltage dependence is that the fluorophore could be affected by molecular events outside the S0 helix.

The S4 transmembrane segment moves relatively to S0 during channel voltage–dependent operation

Given the close association of S0 and S4 (Liu et al., 2008a, 2010), and the complex ΔF/F profile of channels labeled

at position 20 (see above), we hypothesized that the fluorescence deflections observed from the S0 flank could be a result of the voltage-dependent interaction between the fluorophore and the quenching group in another VSD segment, specifically W203 outside S4, as tryptophan residues are able to quench small fluorophores. The quenching effect is based on electron transport from the tryptophan side chain to the excited state of the fluorophore, and it has been exploited to investigate structural properties in other proteins (Mansoor et al., 2002; Islas and Zagotta, 2006), as well as to resolve the structure of the short S3–S4 linker in BK$_{Ca}$ channels (Semenova et al., 2009). A previous fluorometric investigation on the voltage dependence of S4 showed that W203 affects the emission of fluorophores (TMRM or PyMPO), labeling the adjacent position 202 (Savalli et al., 2006). We therefore investigated the effects of mutation W203V on the fluorescence deflections resolved from positions 17, 18, 19, and 20 at the extracellular flank of S0.

When position 18 at the S0 extracellular flank was labeled with TMRM in channels bearing mutation W203V (Fig. 5 A), the amplitude of the depolarization-evoked
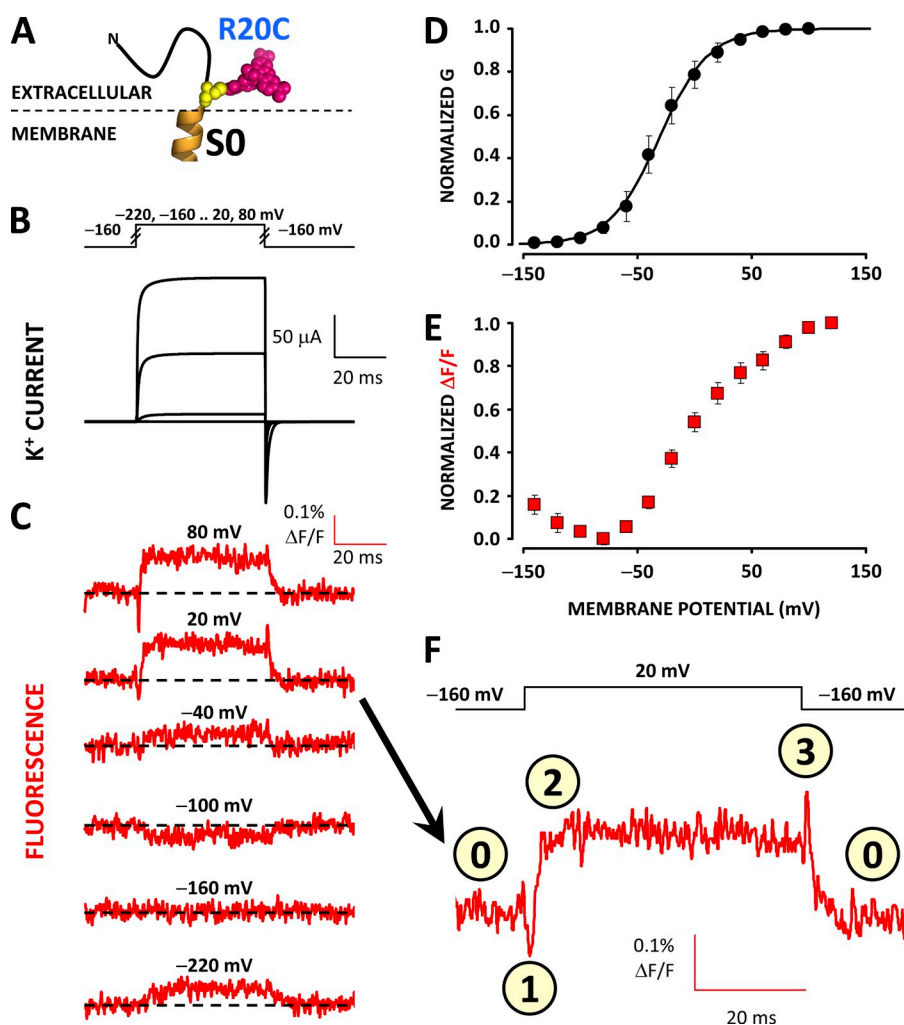

Figure 4. TMRM at position 20 tracks two distinct voltage-dependent processes. (A) A unique cysteine was substituted at position 20 at the putative N-terminal flank of S0 in a BK$_{Ca}$ channel α subunit and covalently labeled with the fluorophore TMRM to resolve conformational rearrangements from this region. (B) Voltage pulses and characteristic evoked K$^+$ currents from BK$_{Ca}$ channels labeled with TMRM at position 20. (C) TMRM fluorescence traces recorded during the voltage pulses in B. Note that, contrary to ΔF/F signals observed from other positions in BK$_{Ca}$, fluorescence recordings to 20 or 80 mV exhibit transient deflections at the onset and termination of the test pulse. (D) Normalized K$^+$ conductance (black circles) fit with a Boltzmann distribution (black curves). Boltzmann parameters are listed in Table I. Error bars represent SEM. (E) Normalized steady-state fluorescence. The biphasic relationship implies that two processes with opposite effects on fluorescence intensity (quenching/dequenching) and steady-state voltage dependence influence TMRM fluorescence when labeling position 20. (F) Magnification of the fluorescence trace for a 20-mV depolarization from C. In this scale, the fluorescence transients (events marked 1 and 3) are more easily observed.

ΔF/F was diminished by an order of magnitude (Fig. 5, B and G). The same was observed when labeling positions 17 and 19 (Fig. 5 G). This result suggests that, at rest, W203 acts as a fluorescence quencher for the fluorophore, labeling the region extracellular to S0. Depolarization evokes a relative motion between the two segments so that the quenching effect is lifted, and a positive ΔF/F is observed. Accordingly, this effect is abolished by mutation W203V. Moreover, in W203V channels labeled at position 20 (Fig. 5 D), the unquenching component is abolished, unmasking the residual quenching process (Fig. 5, E and F).

To confirm tryptophan's ability to quench TMRM fluorescence, we assessed the quenching efficiency of an un-charged L-tryptophan derivative that resembles the structure of nonterminal Trp in proteins (NATA; Fig. 6 A) on TMRM in solution. The concentration-dependent quenching effect of NATA on 1 µM TMRM is shown in Fig. 6 C. The estimated Stern-Volmer quenching constant is 41.3 M^{-1} (Fig. 6 D), within the same order of magnitude as the tryptophan quenching efficiency for bimane fluorescence: 83 M^{-1} (Islas and Zagotta, 2006).

DISCUSSION

The nonconserved BK_{Ca} transmembrane domain S0 and the short extracellular N-terminal tail that precedes it are
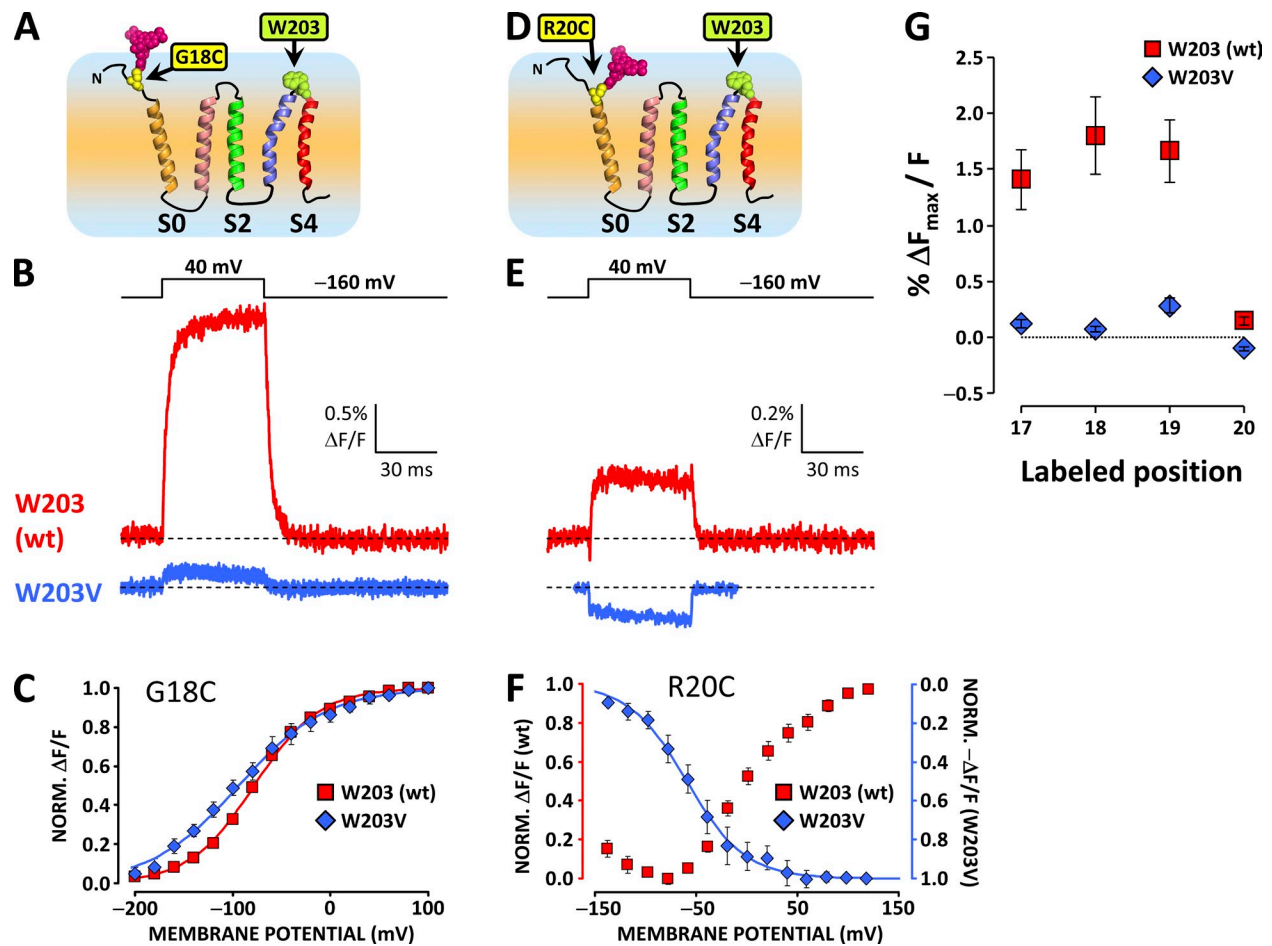

Figure 5. A large component of the ΔF reported from the S0 extracellular flank is abolished by the substitution of W203 at the extracellular tip of S4. (A) Putative topology of the BK_{Ca} channel α subunit voltage sensor domain. A unique cysteine was substituted at position 18 at the putative N-terminal flank of S0 to resolve conformational rearrangements from this region. W203 is also indicated in green. (B) TMRM fluorescence traces recorded during depolarization to 40 mV from wt channels labeled at position 18 (red trace, as in Fig. 2 G) and channels bearing mutation W203V (blue trace). Note the dramatically diminished ΔF/F signal amplitude. (C) Normalized TMRM fluorescence from channels with mutation W203V (blue diamonds) and without (red squares), plotted against membrane potential and fitted with Boltzmann distributions (blue and red curves, respectively). Boltzmann parameters are listed in Table I. Error bars represent SEM. (D–F) As in A–C, respectively, for wt and W203V channels labeled at position 20. In this position, the fluorophore is apparently influenced by two voltage-dependent processes with opposite effects on its fluorescence intensity (Fig. 4). Mutation W203V diminishes the voltage-dependent unquenching process, but it does not apparently affect the residual voltage-dependent quenching process (E). (G) Mean fitted $ΔF_{max}/F$ signal, normalized for fitted maximum conductance to normalize for channel expression, plotted against labeled position, for wt and W203V channels. Mutation W203V diminishes the ΔF/F observed from positions 17–19 by ≈90%. At position 20, mutation W203V removes the unquenching process (positive ΔF/F) to reveal a residual negative ΔF/F signal. Error bars represent SEM.

important for the functional interaction between channel-forming α subunits and regulatory β subunits (Wallner et al., 1996; Morrow et al., 2006). More recently, it was reported that an interaction site could exist between S0 and the voltage-sensing apparatus of BK_{Ca} channels (Koval et al., 2007), whereas S0 was found to associate closely with VSDs S3 and S4, so that disulfide bridge formation between their extracellular regions is highly efficient (Liu et al., 2008a, 2010). Intrigued by this intimate association, we optically investigated voltage-dependent conformational rearrangements from the proximity of S0 (Figs. 2 and 4), testing the hypothesis that S0 undergoes voltage-dependent motions during activation.

Large fluorescence deflections reported from the S0 extracellular flank

The TMRM fluorescence deflections observed from positions immediately extracellular to S0 (17, 18, and 19; Fig. 2) are exceptionally large compared with those resolved from transmembrane segments with intrinsic voltage dependence, S2 and S4 (see ΔF/F amplitude scales in Fig. 3 and Savalli et al., 2006, 2007; Pantazis et al., 2010). When large fluorescence deflections are observed from a contiguous series of labeling positions in a protein segment, it is reasonable to assume that they are a result of an extensive movement of the entire labeled region, as suggested by Pathak et al. (2007). However, we were unable to experimentally establish whether S0 undergoes large movements owing to intrinsic voltage dependence because neutralization of R20 did not perturb the large ΔF/F signal, and R44 mutants could not be investigated. Nevertheless, a clue for the source of the large ΔF/F signal came from the fluorescence signature

of position 20: the composite ΔF/F reported from this location (Fig. 4) indicates that at least two different voltage-dependent processes, with distinct time- and voltage-dependent properties, influence the emission of the attached fluorophore, raising the possibility that the fluorescence emission is perturbed by events outside S0.

A relative motion between S0 and S4 accounts for the optical signal

Indeed, the tryptophan residue at the extracellular tip of S4 (W203) was found to be the principal molecular source of the fluorescence deflections observed from positions 17–20, as mutation W203V abolished most of the depolarization-dependent positive ΔF/F component, while apparently not perturbing the quenching component observed from position 20 (Fig. 5). Therefore, the fluorescence deflections resolved must be primarily a result of the relative motion between W203 (S4) and the fluorophore attached to the extracellular flank of S0. The structural interpretation of these results is that the two segments are within collisional proximity at rest, in agreement with the conclusions of previous investigations (Koval et al., 2007; Liu et al., 2008a, 2010). However, upon VSD reorganization after membrane depolarization, the two segments move apart, relieving the fluorophore of the quenching effect of W203. Based on this interpretation, we present a model accounting for the experimental observations in Fig. 7.

Interpretation of the composite fluorescence signal reported from position 20

We propose a mechanism to account for this complex fluorescence signal, whereupon W203 and another
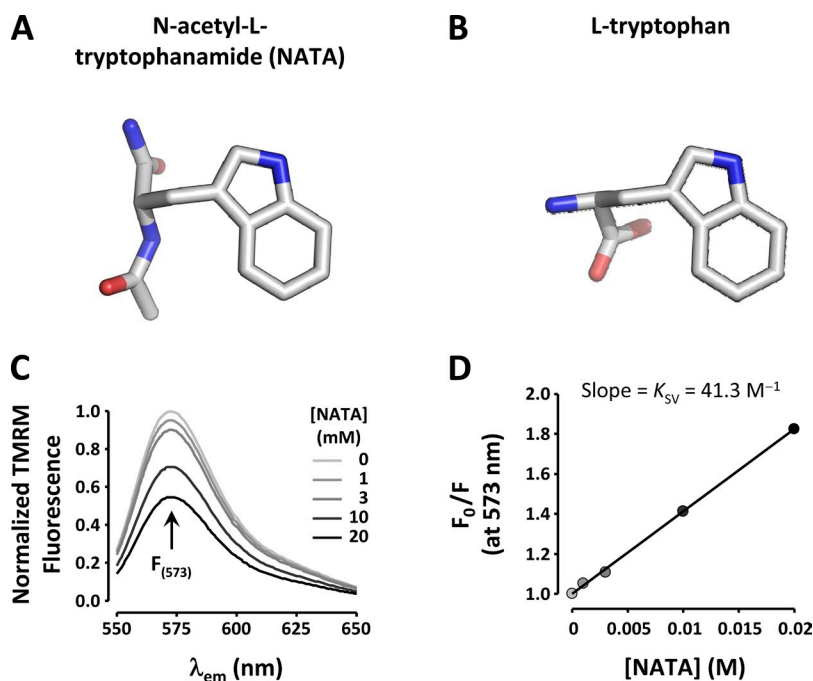

A   N-acetyl-L-tryptophanamide (NATA)

B   L-tryptophan

C

D   Slope = K_{SV} = 41.3 M^{-1}

Figure 6. A tryptophan derivative can quench TMRM in solution. (A) Molecular structure of NATA, an uncharged L-tryptophan derivative that resembles the structure of nonterminal Trp in proteins. (B) The molecular structure of L-tryptophan. (C) Fluorescence spectra of 1 µM TMRM in external solution under increasing [NATA]. (D) Stern-Volmer plot of peak TMRM fluorescence (573 nm) quenched by NATA. The Stern-Volmer constant (K_{SV}) is 41.3 M^{-1}.

quencher influence TMRM fluorescence, giving rise to the observed positive and negative $\Delta F/F$, respectively (Fig. S1). The nature of the second quencher remains unknown. However, because position 20 is thought to be near the membrane, we speculate that the labeling fluorophore is influenced by transitions at the interface of the lipid bilayer and the polar solution. Indeed, this quenching process (negative $\Delta F/F$) is fully unmasked by mutation W203V (Fig. 5 E).

Can additional structural information be inferred from the data?

The positions investigated in this work (17–20 in the S0 extracellular flank) are located in the N-terminal tail of the channel (Wallner et al., 1996; Morrow et al., 2006) and are not thought to be involved in a helical structure (Liu et al., 2008a). Lack of structure in the N-terminal region of the α subunit is compatible with this work. A fluorophore labeling the substituted cysteine in a pro-

tein samples a volume of space that is influenced by the flexibility of the protein backbone it is attached to. If the protein backbone spanning positions 17–19 (in the BK$_{Ca}$ N-terminal tail) were part of an α helix, the residue side chains, and consequently the fluorophore space sampled at each position, would be facing 100° away from each other. However, TMRM labeling positions 17–19 is quenched by W203 with comparable efficiency at rest, so that its depolarization-evoked departure gives rise to fluorescence deflections with similar amplitude and kinetics (Figs. 2 and 5), supporting the view that the protein backbone spanning positions 17–19 is unstructured. In contrast, the W203- and depolarization-dependent unquenching process reported from position 20 is much smaller in amplitude (Fig. 5 G). This result could be explained by a more rigid geometry between positions 19 and 20, thus defining the N-terminal boundary of the S0 helix. Alternatively, the expected proximity of position 20 to the membrane could affect
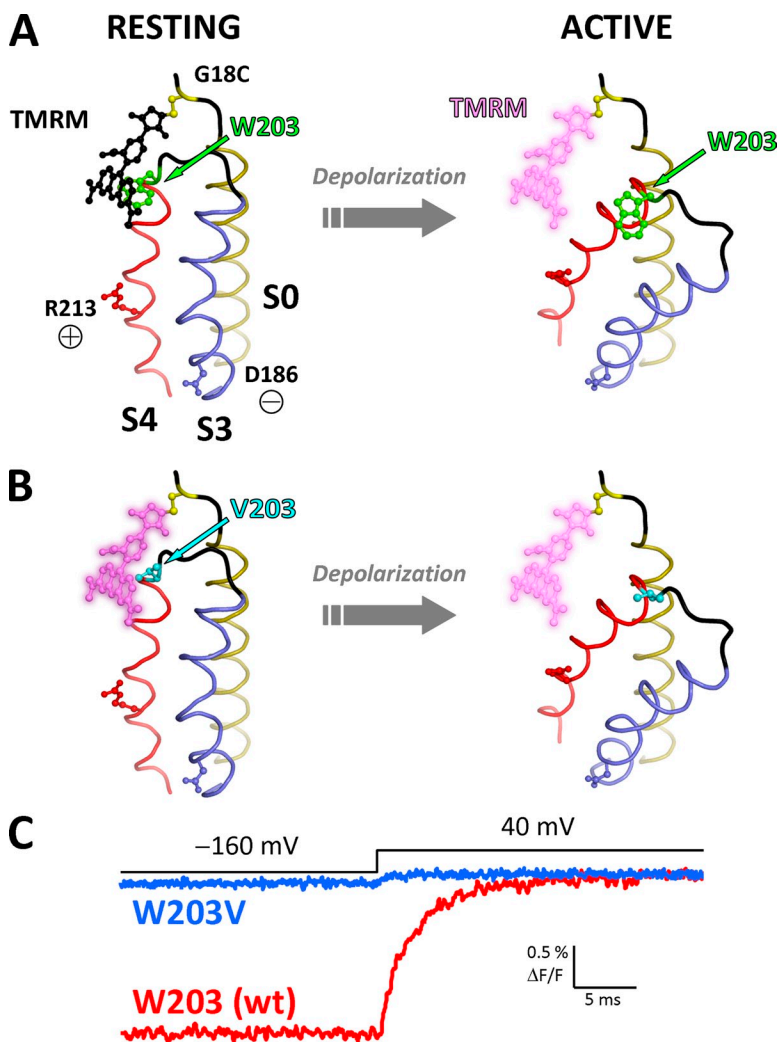

Figure 7. A proposed relative, activation-dependent motion between S0 and S4. (A; left) A hypothetical model of the BK$_{Ca}$ voltage sensor at rest, showing helices S0, S3, and S4 arranged according to the most recent information from disulfide cross-linking efficiency (Liu et al., 2010). S3 (blue) and S4 (red) helices are modeled by homology with the K$_V$1.2-2.1 chimera structure (Protein Data Base accession no. 2R9R) (Long et al., 2007). The two helices are joined by a short helix–loop–helix structure as previously inferred by bimane fluorescence (Semenova et al., 2009). The S0 helix (olive) is modeled as an ideal α helix, whereas its N-terminal flank is shown as a disordered coil (black). A substituted cysteine at position 18 (yellow) is bound by a TMRM molecule (black), which is in close proximity to W203 at the extracellular tip of S4 (green). In this state, TMRM fluorescence is quenched by W203. Voltage-sensing residues D186 (in S3) and R213 (in S4) (Ma et al., 2006) are also shown. (Right) Membrane depolarization induces R213 to move outwards and D186 inwards, causing activation of the voltage sensor domain. This results in a relative motion between the voltage-sensing S3/S4 and S0, increasing the distance between W203 and the fluorophore. As a result, the quenching effect is lifted, producing a large, positive $\Delta F/F$ signal. (B) As in A, for channels with mutation W203V. Because of the absence of W203, TMRM is at a bright state when the VSD is at rest and only exhibits a small deflection during voltage sensor activation. (C) Characteristic TMRM fluorescence traces for wt and W203V channels (red and blue, respectively) labeled at position 18. The traces are superimposed at their fluorescence level when the membrane is depolarized. Fluorescence from wt channels at −160 mV (resting VSD state) is quenched because of the intimate association of the fluorophore with W203 (A). In contrast, the fluorophore is not quenched in W203V channels at rest (B) and emits more fluorescence. TMRM fluorescence in both wt and W203V channels increases upon depolarization after a large or small fluorescence deflection, respectively.

its accessibility for labeling, or the fluorophore at position 20 could simply be further away from W203 at rest, so it is less efficiently quenched. As such, these experiments define a most N-terminal limit for a helical S0 structure at position 19.

Proposed functional relevance of the voltage-dependent divergence of S0 and S4

BK_{Ca} channels possess a "decentralized" distribution of voltage-sensing charged residues across the VSD: two residues in S2 (D153 and R167), one in S3 (D186), and one in S4 (R213) (Ma et al., 2006); indeed, these segments have been demonstrated to undergo voltage-dependent conformational transitions (Savalli et al., 2006, 2007; Pantazis et al., 2010). S1 lacks intrinsic voltage dependence (Ma et al., 2006), whereas the voltage-sensing ability of S0 is unknown as, according to its hydropathy profile, it does not bear membrane-immersed charged residues. Nevertheless, S0 is thought to be a critical component of the BK_{Ca} voltage–sensing apparatus: ΔS0 channels are translated (Wallner et al., 1996; Morrow et al., 2006) but do not produce current—a condition that can be rescued by the coinjection of cRNA encoding S0 (Wallner et al., 1996). Moreover, tryptophan substitution into specific positions in S0 can impair voltage-dependent activation (Koval et al., 2007). By considering the relative voltage-dependent motion between S4 and S0 demonstrated in this work, we propose that S0 could act as a pivot component in the voltage-sensing apparatus of BK_{Ca} channels, against which S4 moves to facilitate channel activation. Furthermore, the transmembrane segments of auxiliary β subunits were recently discovered to localize near segments S0 and S1 (Liu et al., 2008b, 2010; Wu et al., 2009). Association of β subunits with pivot components could in turn affect the structural transitions of voltage-sensitive segments and thus provide a mechanism for channel modulation.

REFERENCES

Armstrong, C.M. 2003. Voltage-gated K channels. *Sci. STKE.* 2003:re10. doi:10.1126/stke.2003.188.re10

Bannister, J.P., B. Chanda, F. Bezanilla, and D.M. Papazian. 2005. Optical detection of rate-determining ion-modulated conformational changes of the ether-à-go-go K+ channel voltage sensor. *Proc. Natl. Acad. Sci. USA.* 102:18718–18723. doi:10.1073/pnas.0505766102

Bao, L., and D.H. Cox. 2005. Gating and ionic currents reveal how the BK_{Ca} channel's Ca^{2+} sensitivity is enhanced by its β1 subunit. *J. Gen. Physiol.* 126:393–412. doi:10.1085/jgp.200509346

Bao, L., C. Kaldany, E.C. Holmstrand, and D.H. Cox. 2004. Mapping the BK_{Ca} channel's "Ca^{2+} bowl": side-chains essential for Ca^{2+} sensing. *J. Gen. Physiol.* 123:475–489. doi:10.1085/jgp.200409052

Bezanilla, F. 2008. How membrane proteins sense voltage. *Nat. Rev. Mol. Cell Biol.* 9:323–332.

Bian, S., I. Favre, and E. Moczydlowski. 2001. Ca2+-binding activity of a COOH-terminal fragment of the Drosophila BK channel involved in Ca2+-dependent activation. *Proc. Natl. Acad. Sci. USA.* 98:4776–4781.

Braun, A.P., and L. Sy. 2001. Contribution of potential EF hand motifs to the calcium-dependent gating of a mouse brain large conductance, calcium-sensitive K(+) channel. *J. Physiol.* 533:681–695. doi:10.1111/j.1469-7793.2001.00681.x

Bruening-Wright, A., F. Elinder, and H.P. Larsson. 2007. Kinetic relationship between the voltage sensor and the activation gate in spHCN channels. *J. Gen. Physiol.* 130:71–81. doi:10.1085/jgp.200709769

Cha, A., and F. Bezanilla. 1997. Characterizing voltage-dependent conformational changes in the Shaker K+ channel with fluorescence. *Neuron.* 19:1127–1140. doi:10.1016/S0896-6273(00)80403-1

Chanda, B., and F. Bezanilla. 2002. Tracking voltage-dependent conformational changes in skeletal muscle sodium channel during activation. *J. Gen. Physiol.* 120:629–645.

Chanda, B., and F. Bezanilla. 2008. A common pathway for charge transport through voltage-sensing domains. *Neuron.* 57:345–351.

Claydon, T.W., and D. Fedida. 2007. Voltage clamp fluorimetry studies of mammalian voltage-gated K(+) channel gating. *Biochem. Soc. Trans.* 35:1080–1082. doi:10.1042/BST0351080

Cui, J. 2010. BK-type calcium-activated potassium channels: coupling of metal ions and voltage sensing. *J. Physiol.* In press.

Cui, J., and R.W. Aldrich. 2000. Allosteric linkage between voltage and Ca(2+)-dependent activation of BK-type mslo1 K(+) channels. *Biochemistry.* 39:15612–15619. doi:10.1021/bi001509+

Cui, J., H. Yang, and U.S. Lee. 2009. Molecular mechanisms of BK channel activation. *Cell. Mol. Life Sci.* 66:852–875.

Díaz, L., P. Meera, J. Amigo, E. Stefani, O. Alvarez, L. Toro, and R. Latorre. 1998. Role of the S4 segment in a voltage-dependent calcium-sensitive potassium (hSlo) channel. *J. Biol. Chem.* 273:32430–32436.

Gandhi, C.S., and E.Y. Isacoff. 2005. Shedding light on membrane proteins. *Trends Neurosci.* 28:472–479. doi:10.1016/j.tins.2005.07.005

Gandhi, C.S., and R. Olcese. 2008. The voltage-clamp fluorometry technique. *In* Methods in Molecular Biology, Potassium Channels. J.D. Lippiat, editor. Humana Press, Totowa, NJ. 213–231.

Haug, T., D. Sigg, S. Ciani, L. Toro, E. Stefani, and R. Olcese. 2004. Regulation of K^+ flow by a ring of negative charges in the outer pore of BK_{Ca} channels. Part I. Aspartate 292 modulates K^+ conduction by external surface charge effect. *J. Gen. Physiol.* 124:173–184. doi:10.1085/jgp.200308949

Horne, A.J., and D. Fedida. 2009. Use of voltage clamp fluorimetry in understanding potassium channel gating: a review of Shaker fluorescence data. *Can. J. Physiol. Pharmacol.* 87:411–418. doi:10.1139/Y09-024

Horne, A.J., C.J. Peters, T.W. Claydon, and D. Fedida. 2010. Fast and slow voltage sensor rearrangements during activation gating in Kv1.2 channels detected using tetramethylrhodamine fluorescence. *J. Gen. Physiol.* 136:83–99.

Horrigan, F.T., and R.W. Aldrich. 2002. Coupling between voltage sensor activation, Ca^{2+} binding and channel opening in large conductance (BK) potassium channels. *J. Gen. Physiol.* 120:267–305.

Hou, S., S.H. Heinemann, and T. Hoshi. 2009. Modulation of BKCa channel gating by endogenous signaling molecules. *Physiology (Bethesda)*. 24:26–35.

Islas, L.D., and W.N. Zagotta. 2006. Short-range molecular rearrangements in ion channels detected by tryptophan quenching of bimane fluorescence. *J. Gen. Physiol.* 128:337–346. doi:10.1085/jgp.200609556

Kohout, S.C., M.H. Ulbrich, S.C. Bell, and E.Y. Isacoff. 2008. Subunit organization and functional transitions in Ci-VSP. *Nat. Struct. Mol. Biol.* 15:106–108. doi:10.1038/nsmb1320

Koval, O.M., Y. Fan, and B.S. Rothberg. 2007. A role for the S0 transmembrane segment in voltage-dependent gating of BK channels. *J. Gen. Physiol.* 129:209–220.

Lakowicz, J.R. 2006. Principles of Fluorescence Spectroscopy. Third edition. Springer, New York. 954 pp.

Latorre, R., and S. Brauchi. 2006. Large conductance Ca2+-activated K+ (BK) channel: activation by Ca2+ and voltage. *Biol. Res.* 39:385–401.

Latorre, R., and C. Miller. 1983. Conduction and selectivity in potassium channels. *J. Membr. Biol.* 71:11–30. doi:10.1007/BF01870671

Latorre, R., F.J. Morera, and C. Zaelzer. 2010. Allosteric interactions and the modular nature of the voltage- and Ca2+-activated (BK) channel. *J. Physiol.* 588:3141–3148. doi:10.1113/jphysiol.2010.191999

Lee, U.S., and J. Cui. 2010. BK channel activation: structural and functional insights. *Trends Neurosci.* 33:415–423.

Liu, G., S.I. Zakharov, L. Yang, S.X. Deng, D.W. Landry, A. Karlin, and S.O. Marx. 2008a. Position and role of the BK channel α subunit S0 helix inferred from disulfide crosslinking. *J. Gen. Physiol.* 131:537–548.

Liu, G., S.I. Zakharov, L. Yang, R.S. Wu, S.X. Deng, D.W. Landry, A. Karlin, and S.O. Marx. 2008b. Locations of the beta1 transmembrane helices in the BK potassium channel. *Proc. Natl. Acad. Sci. USA*. 105:10727–10732.

Liu, G., X. Niu, R.S. Wu, N. Chudasama, Y. Yao, X. Jin, R. Weinberg, S.I. Zakharov, H. Motoike, S.O. Marx, and A. Karlin. 2010. Location of modulatory β subunits in BK potassium channels. *J. Gen. Physiol.* 135:449–459. doi:10.1085/jgp.201010417

Long, S.B., E.B. Campbell, and R. Mackinnon. 2005. Crystal structure of a mammalian voltage-dependent Shaker family K+ channel. *Science*. 309:897–903. doi:10.1126/science.1116269

Long, S.B., X. Tao, E.B. Campbell, and R. MacKinnon. 2007. Atomic structure of a voltage-dependent K+ channel in a lipid membrane-like environment. *Nature*. 450:376–382. doi:10.1038/nature06265

Lu, R., A. Alioua, Y. Kumar, M. Eghbali, E. Stefani, and L. Toro. 2006. MaxiK channel partners: physiological impact. *J. Physiol.* 570:65–72. doi:10.1113/jphysiol.2005.098913

Ma, Z., X.J. Lou, and F.T. Horrigan. 2006. Role of charged residues in the S1–S4 voltage sensor of BK channels. *J. Gen. Physiol.* 127:309–328.

Magleby, K.L. 2003. Gating mechanism of BK (Slo1) channels: so near, yet so far. *J. Gen. Physiol.* 121:81–96.

Mannuzzu, L.M., M.M. Moronne, and E.Y. Isacoff. 1996. Direct physical measure of conformational rearrangement underlying potassium channel gating. *Science*. 271:213–216. doi:10.1126/science.271.5246.213

Mansoor, S.E., H.S. McHaourab, and D.L. Farrens. 2002. Mapping proximity within proteins using fluorescence spectroscopy. A study of T4 lysozyme showing that tryptophan residues quench bimane fluorescence. *Biochemistry*. 41:2475–2484. doi:10.1021/bi011198i

Meera, P., M. Wallner, M. Song, and L. Toro. 1997. Large conductance voltage- and calcium-dependent K+ channel, a distinct member of voltage-dependent ion channels with seven N-terminal transmembrane segments (S0-S6), an extracellular N terminus, and an intracellular (S9-S10) C terminus. *Proc. Natl. Acad. Sci. USA*. 94:14066–14071. doi:10.1073/pnas.94.25.14066

Morrow, J.P., S.I. Zakharov, G. Liu, L. Yang, A.J. Sok, and S.O. Marx. 2006. Defining the BK channel domains required for beta1-subunit modulation. *Proc. Natl. Acad. Sci. USA*. 103:5096–5101.

Orio, P., and R. Latorre. 2005. Differential effects of β1 and β2 subunits on BK channel activity. *J. Gen. Physiol.* 125:395–411.

Orio, P., P. Rojas, G. Ferreira, and R. Latorre. 2002. New disguises for an old channel: MaxiK channel beta-subunits. *News Physiol. Sci.* 17:156–161.

Orio, P., Y. Torres, P. Rojas, I. Carvacho, M.L. Garcia, L. Toro, M.A. Valverde, and R. Latorre. 2006. Structural determinants for functional coupling between the β and α subunits in the Ca^{2+}-activated K^+ (BK) channel. *J. Gen. Physiol.* 127:191–204. doi:10.1085/jgp.200509370

Pantazis, A., V. Gudzenko, N. Savalli, D. Sigg, and R. Olcese. 2010. Operation of the voltage sensor of a human voltage- and Ca2+-activated K+ channel. *Proc. Natl. Acad. Sci. USA*. 107:4459–4464. doi:10.1073/pnas.0911959107

Pathak, M.M., V. Yarov-Yarovoy, G. Agarwal, B. Roux, P. Barth, S. Kohout, F. Tombola, and E.Y. Isacoff. 2007. Closing in on the resting state of the Shaker K(+) channel. *Neuron*. 56:124–140.

Rothberg, B.S., and K.L. Magleby. 2000. Voltage and Ca^{2+} activation of single large-conductance Ca^{2+}-activated K^+ channels described by a two-tiered allosteric gating mechanism. *J. Gen. Physiol.* 116:75–99.

Salkoff, L., A. Butler, G. Ferreira, C. Santi, and A. Wei. 2006. High-conductance potassium channels of the SLO family. *Nat. Rev. Neurosci.* 7:921–931. doi:10.1038/nrn1992

Savalli, N., A. Kondratiev, L. Toro, and R. Olcese. 2006. Voltage-dependent conformational changes in human Ca(2+)- and voltage-activated K(+) channel, revealed by voltage-clamp fluorometry. *Proc. Natl. Acad. Sci. USA*. 103:12619–12624. doi:10.1073/pnas.0601176103

Savalli, N., A. Kondratiev, S.B. de Quintana, L. Toro, and R. Olcese. 2007. Modes of operation of the BK_{Ca} channel $β_2$ subunit. *J. Gen. Physiol.* 130:117–131. doi:10.1085/jgp.200709803

Schreiber, M., and L. Salkoff. 1997. A novel calcium-sensing domain in the BK channel. *Biophys. J.* 73:1355–1363.

Semenova, N.P., K. Abarca-Heidemann, E. Loranc, and B.S. Rothberg. 2009. Bimane fluorescence scanning suggests secondary structure near the S3-S4 linker of BK channels. *J. Biol. Chem.* 284:10684–10693.

Sheng, J.Z., A. Weljie, L. Sy, S. Ling, H.J. Vogel, and A.P. Braun. 2005. Homology modeling identifies C-terminal residues that contribute to the Ca2+ sensitivity of a BKCa channel. *Biophys. J.* 89:3079–3092. doi:10.1529/biophysj.105.063610

Smith, P.L., and G. Yellen. 2002. Fast and slow voltage sensor movements in HERG potassium channels. *J. Gen. Physiol.* 119:275–293. doi:10.1085/jgp.119.3.275

Stefani, E., and F. Bezanilla. 1998. Cut-open oocyte voltage-clamp technique. *Methods Enzymol.* 293:300–318. doi:10.1016/S0076-6879(98)93020-8

Stefani, E., M. Ottolia, F. Noceti, R. Olcese, M. Wallner, R. Latorre, and L. Toro. 1997. Voltage-controlled gating in a large conductance Ca2+-sensitive K+channel (hslo). *Proc. Natl. Acad. Sci. USA*. 94:5427–5431.

Swartz, K.J. 2004. Towards a structural view of gating in potassium channels. *Nat. Rev. Neurosci.* 5:905–916.

Swartz, K.J. 2008. Sensing voltage across lipid membranes. *Nature*. 456:891–897. doi:10.1038/nature07620

Sweet, T.B., and D.H. Cox. 2008. Measurements of the BK_{Ca} channel's high-affinity Ca^{2+} binding constants: effects of membrane voltage. *J. Gen. Physiol.* 132:491–505. doi:10.1085/jgp.200810094

Sweet, T.B., and D.H. Cox. 2009. Measuring the influence of the BK_{Ca} β1 subunit on Ca^{2+} binding to the BK_{Ca} channel. *J. Gen. Physiol.* 133:139–150. doi:10.1085/jgp.200810129

Tombola, F., M.M. Pathak, and E.Y. Isacoff. 2006. How does voltage open an ion channel? *Annu. Rev. Cell Dev. Biol.* 22:23–52.

Tombola, F., M.H. Ulbrich, S.C. Kohout, and E.Y. Isacoff. 2010. The opening of the two pores of the Hv1 voltage-gated proton channel is tuned by cooperativity. *Nat. Struct. Mol. Biol.* 17:44–50.

Toro, L., M. Wallner, P. Meera, and Y. Tanaka. 1998. Maxi-K(Ca), a unique member of the voltage-gated K channel superfamily. *News Physiol. Sci.* 13:112–117.

Vaid, M., T.W. Claydon, S. Rezazadeh, and D. Fedida. 2008. Voltage clamp fluorimetry reveals a novel outer pore instability in a mammalian voltage-gated potassium channel. *J. Gen. Physiol.* 132:209–222. doi:10.1085/jgp.200809978

Villalba-Galea, C.A., W. Sandtner, D.M. Starace, and F. Bezanilla. 2008. S4-based voltage sensors have three major conformations. *Proc. Natl. Acad. Sci. USA.* 105:17600–17607. doi:10.1073/pnas.0807387105

Wallner, M., P. Meera, M. Ottolia, G.J. Kaczorowski, R. Latorre, M.L. Garcia, E. Stefani, and L. Toro. 1995. Characterization of and modulation by a beta-subunit of a human maxi KCa channel cloned from myometrium. *Receptors Channels.* 3:185–199.

Wallner, M., P. Meera, and L. Toro. 1996. Determinant for beta-subunit regulation in high-conductance voltage-activated and Ca(2+)-sensitive K+ channels: an additional transmembrane region at the N terminus. *Proc. Natl. Acad. Sci. USA.* 93:14922–14927.

Wang, L., and F.J. Sigworth. 2009. Structure of the BK potassium channel in a lipid membrane from electron cryomicroscopy. *Nature.* 461:292–295. doi:10.1038/nature08291

Wei, A., C. Solaro, C. Lingle, and L. Salkoff. 1994. Calcium sensitivity of BK-type KCa channels determined by a separable domain. *Neuron.* 13:671–681. doi:10.1016/0896-6273(94)90034-5

Wu, R.S., and S.O. Marx. 2010. The BK potassium channel in the vascular smooth muscle and kidney: α- and β-subunits. *Kidney Int.* 78:963–974.

Wu, R.S., N. Chudasama, S.I. Zakharov, D. Doshi, H. Motoike, G. Liu, Y. Yao, X. Niu, S.X. Deng, D.W. Landry, et al. 2009. Location of the beta 4 transmembrane helices in the BK potassium channel. *J. Neurosci.* 29:8321–8328. doi:10.1523/JNEUROSCI.6191-08.2009

Wu, Y., Y. Yang, S. Ye, and Y. Jiang. 2010. Structure of the gating ring from the human large-conductance Ca(2+)-gated K(+) channel. *Nature.* 466:393–397.

Xia, X.M., X. Zeng, and C.J. Lingle. 2002. Multiple regulatory sites in large-conductance calcium-activated potassium channels. *Nature.* 418:880–884. doi:10.1038/nature00956

Yang, J., G. Krishnamoorthy, A. Saxena, G. Zhang, J. Shi, H. Yang, K. Delaloye, D. Sept, and J. Cui. 2010. An epilepsy/dyskinesia-associated mutation enhances BK channel activation by potentiating Ca2+ sensing. *Neuron.* 66:871–883. doi:10.1016/j.neuron.2010.05.009

Yuan, P., M.D. Leonetti, A.R. Pico, Y. Hsiung, and R. MacKinnon. 2010. Structure of the human BK channel Ca2+-activation apparatus at 3.0 Å resolution. *Science.* 329:182–186. doi:10.1126/science.1190414

Yusifov, T., N. Savalli, C.S. Gandhi, M. Ottolia, and R. Olcese. 2008. The RCK2 domain of the human BKCa channel is a calcium sensor. *Proc. Natl. Acad. Sci. USA.* 105:376–381.

Yusifov, T., A.D. Javaherian, A. Pantazis, C.S. Gandhi, and R. Olcese. 2010. The RCK1 domain of the human BK_{Ca} channel transduces Ca^{2+} binding into structural rearrangements. *J. Gen. Physiol.* 136:189–202.

Zeng, X.H., X.M. Xia, and C.J. Lingle. 2005. Divalent cation sensitivity of BK channel activation supports the existence of three distinct binding sites. *J. Gen. Physiol.* 125:273–286. doi:10.1085/jgp.200409239